Spontaneous emission of gravity waves in the differentially heated rotating annulus

S. Borchert [1*], U. Achatz [1], M. D. Fruman [1]

[1] Institut für Atmosphäre und Umwelt, Goethe-Universität Frankfurt, Frankfurt (Main), Germany

*Contact: borchert@iau.uni-frankfurt.de

MetStröm

Introduction

Gravity waves (GWs) play an important role in atmospheric dynamics by transporting momentum over considerable distances, affecting daily weather as well as the climate. Spontaneous GW emission by imbalances of the large-scale flow may be an important source of GWs in the atmosphere and no satisfactory parameterization in weather and climate models for it exists [1].
In trying to obtain further insight into this process, the differentially heated rotating annulus experiment might serve as a complement to observations in the atmosphere. Experiments with a rotating annulus exhibiting a jet modulated by large-scale waves arising due to baroclinic instability have already been used to study GWs: Williams et al. [2] observed small-scale interfacial waves in a two-layer flow, and Jacoby et al. [3] detected GWs emitted from boundary-layer instabilities in a differentially heated annulus.
In order to study if the differentially heated rotating annulus might be useful for the investigation of spontaneous GW emission, we employ a finite-volume model (cylFloit) [4].

Model

The annulus experiment consists of 2 coaxial cylinders mounted on a rotating table. The inner cylinder is cooled to a temperature T_a and the outer cylinder is heated to T_b ($T_a < T_b$). The gap between the cylinders is filled with the working fluid, and the whole apparatus rotates at angular velocity Ω (fig. 1).
The numerical model cylFloit is based on the following elements:

- fluid flow is governed by Boussinesq equations [5]

$$\frac{\mathrm{D}\boldsymbol{v}}{\mathrm{D}t} + 2\boldsymbol{\Omega}\times\boldsymbol{v} + \boldsymbol{\Omega}\times(\boldsymbol{\Omega}\times\boldsymbol{r}) + \frac{\mathrm{d}\boldsymbol{\Omega}}{\mathrm{d}t}\times\boldsymbol{r} = \tilde{\rho}\boldsymbol{g} - \boldsymbol{\nabla}\cdot\mathbb{P},$$
$$\frac{\mathrm{D}T}{\mathrm{D}t} = \boldsymbol{\nabla}\cdot(\kappa\boldsymbol{\nabla}T),$$
$$\boldsymbol{\nabla}\cdot\boldsymbol{v} = 0,$$

  with velocity $\boldsymbol{v}$, position $\boldsymbol{r}$, density deviation $\tilde{\rho} = \tilde{\rho}(T) = (\rho - \rho_0)/\rho_0$, reduced gravity $\tilde{\rho}\boldsymbol{g}$, molecular momentum flux $\mathbb{P} = \tilde{p}\,\mathbb{I} - \nu\left[\boldsymbol{\nabla}\boldsymbol{v} + (\boldsymbol{\nabla}\boldsymbol{v})^{\mathrm{T}}\right]$, pressure deviation $\tilde{p} = (p - p_0)/\rho_0$, unit tensor $\mathbb{I}$, kinematic viscosity $\nu = \nu(T)$ and thermal diffusivity $\kappa = \kappa(T)$
- finite-volume discretization on regular, cylindrical C-grid (fig. 1)
- implicit parameterization of subgrid-scale turbulence by Adaptive Local Deconvolution Method (ALDM) [6]
- validation against laboratory measurements provided by U. Harlander (BTU Cottbus-Senftenberg) [5, 7]

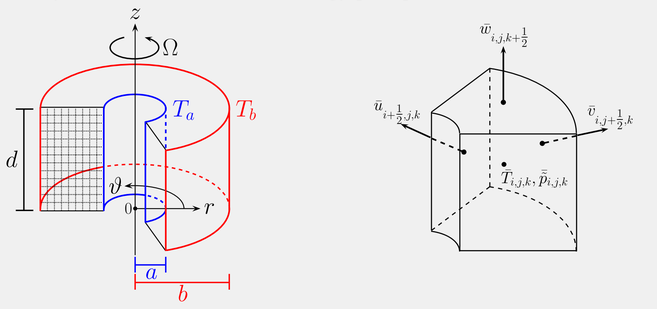

Figure 1. *Left*: Schematic view of differentially heated rotating annulus with sector removed to indicate cell walls of regular, cylindrical finite-volume grid (dotted lines). *Right*: Arrangement of variables in finite-volume grid cell.

Atmosphere-like annulus configuration

The ratio of the Brunt-Väisälä frequency N to the Coriolis parameter $f = 2\Omega$ is an important parameter for the GW propagation. Its value in classical annulus configurations [e.g. 8] is $N/f \sim 0.1$, compared to $N/f \sim 100$ in the atmosphere.
Using the global estimate

$$N \approx \sqrt{\frac{g\alpha\,(T_b - T_a)}{d}},$$

with expansion coefficient α, a more atmosphere-like annulus configuration has been chosen as test bed. Its parameters are listed in tab. 1. This configuration features (see fig. 2):

Table 1. Atmosphere-like annulus parameters

Radius of inner cylinder:	$a = 20\,\mathrm{cm}$
Radius of outer cylinder:	$b = 70\,\mathrm{cm}$
Fluid depth:	$d = 4\,\mathrm{cm}$
Temperature difference:	$T_b - T_a = 30\,\mathrm{K}$
Angular velocity:	$\Omega = 0.76\,\mathrm{rpm}$
Working fluid:	water

- baroclinic wave of azimuthal mode number 3
- $N/f > 1$
- spiral-like GW pattern within baroclinic wave as indicated by horizontal velocity divergence $\delta = \boldsymbol{\nabla_h}\cdot\boldsymbol{u}$ (with horizontal velocity component $\boldsymbol{u}$) [9]

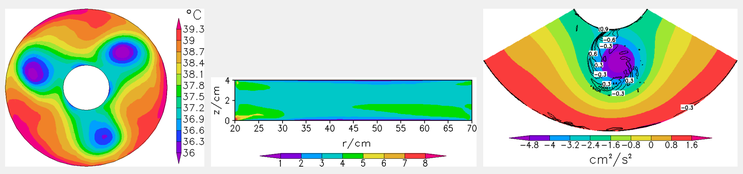

Figure 2. *Left*: Horizontal cross section of temperature at mid-height ($z = 2\,\mathrm{cm}$). *Centre*: Vertical cross section of azimuthally averaged N/f. *Right*: Pressure (colors) and contours of horizontal velocity divergence in $10^{-1}\,\mathrm{s}^{-1}$ (black) of one lobe of baroclinic wave.

Indicators of GW activity

Linear modal decomposition

Linear theory is used to estimate the contribution of the GWs to the small-scale structures of the flow. The method consists of:

- large-scale part of velocity, buoyancy and pressure fields: $\overline{\boldsymbol{X}} := (\overline{\boldsymbol{v}}, \bar{B} = -\bar{\tilde{\rho}}g, \bar{\tilde{p}})$ is obtained from moving average
- within averaging volume Fourier decomposition of small-scale part: $\boldsymbol{X}' = \boldsymbol{X} - \overline{\boldsymbol{X}} \to \widehat{\boldsymbol{X}}_{k,l,m}$ (with azimuthal, radial and vertical wave numbers k, l and m which are omitted in the following)
- express small-scale part as superposition of geostrophic mode $\widehat{\boldsymbol{R}}$ and GW modes $\widehat{\boldsymbol{G}}^{\pm}$: $\widehat{\boldsymbol{X}} = \varrho\widehat{\boldsymbol{R}} + \gamma^{+}\widehat{\boldsymbol{G}}^{+} + \gamma^{-}\widehat{\boldsymbol{G}}^{-}$
- modes are orthonormal with respect to energy scalar product: $\langle\widehat{\boldsymbol{X}}_1, \widehat{\boldsymbol{X}}_2\rangle := (\hat{\boldsymbol{v}}_1\cdot\hat{\boldsymbol{v}}_2^{*} + \hat{B}_1\hat{B}_2^{*}/N^2)/2$ (* denotes complex conjugate)
- thus total energy of $\widehat{\boldsymbol{X}}$ is: $\langle\widehat{\boldsymbol{X}}, \widehat{\boldsymbol{X}}\rangle = |\varrho|^2 + |\gamma^{+}|^2 + |\gamma^{-}|^2$, and modal contributions obtained by projection, e.g. $\varrho = \langle\widehat{\boldsymbol{R}}, \widehat{\boldsymbol{X}}\rangle$
- geostrophic and GW contributions to total energy: $E(\widehat{\boldsymbol{R}}) = \sum_{k,l,m}|\varrho_{k,l,m}|^2$ and $E(\widehat{\boldsymbol{G}}^{\pm}) = \sum_{k,l,m}(|\gamma^{+}_{k,l,m}|^2 + |\gamma^{-}_{k,l,m}|^2)$ are determined grid cell by grid cell, yielding spatially varying energetic decomposition shown in fig. 3

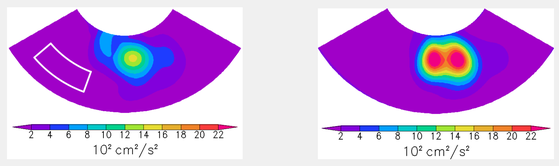

Figure 3. *Left*: Energy contained in the geostrophic mode $E(\widehat{\boldsymbol{R}})$ at mid-hight. White contour indicates approximate horizontal size of volume used for moving average and linear analysis. *Right*: Energy contained in the two GW modes $E(\widehat{\boldsymbol{G}}^{\pm})$.

Unbalanced flow component

The predominant model concept for the investigation of GWs is the decomposition of the flow into balanced (subscript bal) and unbalanced (subscript $unbal$) parts, assuming the latter part to contain the GWs [e.g. 10]

$$\begin{pmatrix}\boldsymbol{v}\\ B\\ \tilde{p}\end{pmatrix} = \begin{pmatrix}\boldsymbol{v}\\ B\\ \tilde{p}\end{pmatrix}_{bal} + \begin{pmatrix}\boldsymbol{v}\\ B\\ \tilde{p}\end{pmatrix}_{unbal}.$$

The decomposition is generally defined through diagnostic balance conditions, which the balanced part of the flow is assumed to satisfy. The accuracy of these conditions may be measured by expressing the magnitude of the unbalanced part of the flow in powers of the Rossby number: $Ro = U/(fL)$ with horizontal velocity and length scales U and L (the decomposition into geostrophic and ageostrophic flow parts is e.g. of order Ro).
A common example of a GW indicator is the horizontal velocity divergence δ. It is based on the assumption that the balanced part of the horizontal velocity field is nondivergent (e.g. a property of the geostrophic flow).
Indicators of higher-order accuracy may be obtained from the GW-filtering constraints [11, 12]

$$\frac{\mathrm{D}^n\delta}{\mathrm{D}t^n} \equiv 0 \quad\text{and}\quad \frac{\mathrm{D}^{n+1}\delta}{\mathrm{D}t^{n+1}} \equiv 0,$$

where $n \in \mathbb{N}_0$. Using the governing equations, the two constraints can be reformulated as two diagnostic balance conditions. Their accuracy should increase with increasing n. For $n = 0$ the balanced part of the flow is nondivergent $\delta = \boldsymbol{\nabla_h}\cdot\boldsymbol{u} \equiv 0$ and satisfies the nonlinear balance equation

$$\Delta\mathrm{NBE} := -(\boldsymbol{\nabla_h}\boldsymbol{u} \cdot\cdot \boldsymbol{\nabla_h}\boldsymbol{u})_{\delta=0} + f\zeta - \nabla_h^2\tilde{p} \equiv 0$$

whith the double scalar product of the horizontal velocity gradient with itself at vanishing divergence $(\boldsymbol{\nabla_h}\boldsymbol{u} \cdot\cdot \boldsymbol{\nabla_h}\boldsymbol{u})_{\delta=0}$ [†] and the vertical component of vorticity $\zeta = \boldsymbol{e_z}\cdot(\boldsymbol{\nabla_h}\times\boldsymbol{u})$.
$\Delta\mathrm{NBE}$ is the residual of the nonlinear balance equation. Regions where $\Delta\mathrm{NBE} \neq 0$ are due to flow imbalances and indicate GW activity [13].

Results

δ and $\Delta\mathrm{NBE}$ show activity close to the inner cylinder wall (see fig. 4). This might be due to GWs originating from boundary layer instabilities described by Jacoby et al. [3]. In addition GW activity is indicated within the baroclinic wave (the spiral-like pattern), which is supported by the results from linear theory (fig. 3). A portion of these GWs might be emitted spontaneously by the large-scale flow of the baroclinic wave.

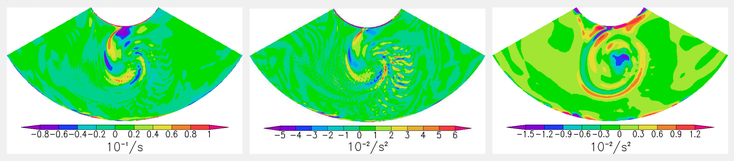

Figure 4. *Left*: Horizontal velocity divergence δ. *Centre*: Residual of nonlinear balance equation $\Delta\mathrm{NBE}$. *Right*: Geostrophic forcing of δ.

[†] The double scalar product of two tensors might be demonstrated using the example of dyads. Given two dyads $\boldsymbol{ab}$ and $\boldsymbol{cd}$, the double scalar product of the two is defined as $\boldsymbol{ab}\cdot\cdot\boldsymbol{cd} = \boldsymbol{a}\cdot(\boldsymbol{b}\cdot\boldsymbol{cd}) = \boldsymbol{b}\cdot\boldsymbol{cd}\cdot\boldsymbol{a}$.

Spontaneous GW emission

A simple model is used to diagnose spontaneous GW emission. It is based on the following elements:

- decomposition of flow into background (subscript 0), geostrophic/hydrostatic (subscript g) and ageostrophic (subscript a) parts

$$\begin{pmatrix}\boldsymbol{v}\\ B\\ \tilde{p}\end{pmatrix} = \begin{pmatrix}0\\ B\\ \tilde{p}\end{pmatrix}_0 + \begin{pmatrix}\boldsymbol{u}\\ B\\ \tilde{p}\end{pmatrix}_g + \begin{pmatrix}\boldsymbol{v}\\ B\\ \tilde{p}\end{pmatrix}_a.$$

- balanced part of flow is given by

$$\frac{\mathrm{d}B_0}{\mathrm{d}z} = \frac{\mathrm{d}^2\tilde{p}_0}{\mathrm{d}z^2} = N^2 = \text{const.}, \quad f\boldsymbol{e_z}\times\boldsymbol{u_g} = \boldsymbol{\nabla_h}\tilde{p}_g \quad\text{and}\quad B_g = \frac{\partial\tilde{p}_g}{\partial z}$$

- to close definition of balanced part, $\tilde{p}_g$ is related diagnostically to quasi-geostrophic potential vorticity $\Pi = \zeta + (f/N^2)\partial B/\partial z$, which is assumed to govern the balanced flow ($\Pi_a \equiv 0$) [14]

$$\left(\nabla_h^2 + \frac{f^2}{N^2}\frac{\partial^2}{\partial z^2}\right)\tilde{p}_g = f\Pi$$

- purely geostrophic forcing of ageostrophic flow is used to diagnose spontaneous GW emission, example: prognostic equation of $\delta = \boldsymbol{\nabla_h}\cdot\boldsymbol{u} = \boldsymbol{\nabla_h}\cdot\boldsymbol{u_a}$

$$\frac{\mathrm{D}\delta}{\mathrm{D}t} = \frac{\partial\boldsymbol{v}}{\partial z}\cdot\boldsymbol{\nabla}w_a - \frac{\partial B_a}{\partial z} + \frac{\partial^2\tilde{p}_{aa}}{\partial z^2} \underbrace{- \frac{\partial^2}{\partial z^2}\nabla^{-2}\left(\boldsymbol{\nabla_h}\boldsymbol{u_g} \cdot\cdot \boldsymbol{\nabla_h}\boldsymbol{u_g}\right)}_{=\frac{\partial^2\tilde{p}_{ag}}{\partial z^2},\ \text{geostrophic forcing}}$$

  with vertical velocity component $w = w_a$ and decomposition of ageostrophic pressure into ageostrophically and geostrophically forced parts $\tilde{p}_a = \tilde{p}_{aa} + \tilde{p}_{ag}$

Results

The purely geostrophic forcing of δ is shown in fig. 4. Stronger activity can be observed close to the inner cylinder wall and within the baroclinic wave. Since viscosity is not included in this simple model of spontaneous GW emission, the signals close to the walls are not reliable. The signals within the baroclinic wave, however, suggest that GW emission is present.

Summary

- finite-volume model of differentially heated rotating annulus (cylFloit) is used for investigation of spontaneous GW emission
- a more atmosphere-like annulus configuration featuring $N/f > 1$ has been chosen as test bed
- clear GW activity is indicated by linear modal decomposition, horizontal velocity divergence δ and residual of nonlinear balance equation $\Delta\mathrm{NBE}$
- purely geostrophic forcing of ageostrophic part of flow indicates that part of GWs in rotating annulus is spontaneously emitted from large-scale flow of baroclinic wave
- next step: use tangent-linear model to quantify contribution of spontaneous emission to GW field [15, 16]

Acknowledgement

The authors are grateful to the German Research Foundation (Deutsche Forschungsgemeinschaft) for partial support through the MetStröm Priority Research Program (Spp 1276), and through grant Ac71/4-2.

References

[1] D. C. Fritts and M. J. Alexander. Gravity wave dynamics and effects in the middle atmosphere. *Rev. Geophys.*, 41 (1):1003, 2003.

[2] P. D. Williams, T. W. N. Haine, and P. L. Read. Inertia-gravity waves emitted from balanced flow: observations, properties, and consequences. *J. Atmos. Sci.*, 65:3543–3556, 2008.

[3] T. N. L. Jacoby, P. L. Read, P. D. Williams, and R. M. B. Young. Generation of inertia-gravity waves in the rotating thermal annulus by a localised boundary layer instability. *Geophys. Astrophys. Fluid Dyn.*, 105:161–181, 2011.

[4] S. Borchert, U. Achatz, and M. D. Fruman. Spontaneous gravity wave emission in the differentially heated rotating annulus. *J. Fluid Mech.*, . submitted.

[5] S. Borchert, U. Achatz, S. Remmler, S. Hickel, U. Harlander, M. Vincze, K. D. Alexandrov, F. Rieper, T. Heppelmann, and S. I. Dolaptchiev. Finite-volume models with implicit subgrid-scale parameterization for the differentially heated rotating annulus. *Meteorol. Z.*, . submitted.

[6] S. Hickel, N. A. Adams, and J. A. Domaradzki. An adaptive local deconvolution method for implicit LES. *J. Comp. Phys.*, 213:413–436, 2006.

[7] M. Vincze, S. Borchert, U. Achatz, Th. von Larcher, M. Baumann, C. Hertel, S. Remmler, T. Beck, K. Alexandrov, Ch. Egbers, J. Fröhlich, V. Heuveline, S. Hickel, and U. Harlander. Benchmarking in a rotating annulus: a comparative experimental and numerical study of baroclinic wave dynamics. *Meteorol. Z.* submitted.

[8] U. Harlander, Th. von Larcher, Y. Wang, and Ch. Egbers. PIV- and LDV-measurements of baroclinic wave interactions in a thermally driven rotating annulus. *Exp. Fluids*, 51(1):37–49, 2011.

[9] D. O'Sullivan and T. J. Dunkerton. Generation of inertia-gravity waves in a simulated life cycle of baroclinic instability. *J. Atmos. Sci.*, 52:3695–3716, 1995.

[10] R. Plougonven and F. Zhang. On the forcing of inertia-gravity waves by synoptic-scale flows. *J. Atmos. Sci.*, 64: 1737–1742, 2007.

[11] K. Hinkelmann. Noncharacteristic filtering of meteorological noise waves. *Contr. Atmos. Phys.*, 35:252–276, 1962.

[12] K. Hinkelmann. Das Filterproblem in der numerischen Wettervorhersage (The filtering problem in numerical weather prediction). *Arch. Meteor. Geoph. Biokl., Ser. A, Suppl. 1*, pages 74–87, 1966.

[13] F. Zhang, S. E. Koch, C. A. Davis, and M. L. Kaplan. A survey of unbalanced flow diagnostics and their application. *Adv. Atmos. Sci.*, 17:165–183, 2000.

[14] T. Warn, O. Bokhove andT. G. Shepherd, and G. K. Vallis. Rossby number expansions, slaving principles, and balance dynamics. *Quart. J. R. Met. Soc.*, 121:723–739, 1995.

[15] C. Snyder, R. Plougonven, and D. J. Muraki. Mechanisms for spontaneous gravity wave generation within a dipole vortex. *J. Atmos. Sci.*, 66:3464–3478, 2009.

[16] S. Wang and F. Zhang. Source of gravity waves within a vortex-dipole jet revealed by a linear model. *J. Atmos. Sci.*, 67:1438–1455, 2010.